JBUON 2013; 18(4): 928-934
ISSN: 1107-0625, online ISSN: 2241-6293 • www.jbuon.com
E-mail: editorial_office@jbuon.com

ORIGINAL ARTICLE

Differential diagnosis of pulmonary lesions by parametric imaging in ^{18}F-FDG PET/CT dynamic multi-bed scanning

Qiang Wang[1], Rong-fu Wang[1], Jianhua-Zhang[1], Yun Zhou[2]

[1]*Department of Nuclear Medicine, Peking University First Hospital, Xichengqu, West District, Beijing, P. R. of China;* [2]*The Russell H. Morgan, Department of Radiology and Radiological Science, Johns Hopkins University, School of Medicine, Baltimore, USA*

Summary

Purpose: *Benign and malignant pulmonary lesions are not easy to distinguish in a clinical setting. We investigated the feasibility of using parametric imaging of the rate constant Ki to diagnose the nature of pulmonary lesions.*

Methods: *Dynamic multi-bed scanning followed by a routine examination was performed on 21 patients with pulmonary lesions who were divided into two groups with malignant or benign lesions based on biopsy and follow-up. The number of patients in the malignant and benign groups were 10 with 15 lesions and 11 with 14 lesions, respectively. The left ventricular blood pool was used for an image-derived input function. The influx rate constant Ki of the pulmonary lesions and parametric images was generated with the Patlak plot method, and the inter-group differences for Ki, maximum standardized uptake value (SUV_{max}), and the time-activity curves (TAC) of fluorine-18-fludeoxyglucose (^{18}F-FDG) were analyzed. At the same time, we investigated the correlation of Ki to SUV_{max}.*

Results: *The maximum diameters of the pulmonary lesions were not significantly different between the malignant and benign groups ($p>0.05$). Ki and SUV_{max} were significantly higher in malignant lesions compared to benign lesions ($p<0.05$). Ki was highly correlated with SUV_{max} in pulmonary lesions ($r=0.815$, $p<0.01$). The malignant lesions showed gradually increasing TAC, and benign lesions exhibited gradually decreasing curves. The parametric images of Ki were useful to distinguish malignant lesions from normal tissue.*

Conclusion: *Our results indicate that Ki parametric imaging in ^{18}F-FDG PET/computed tomography (CT) dynamic multi-bed scanning may be useful in the differential diagnosis of pulmonary lesions.*

Key words: *cancer, diagnosis, ^{18}F-FDG PET/CT , parametric imaging, pulmonary lesions*

Introduction

Fluorine-18-fludeoxyglucose positron emission tomography/computed tomography (^{18}F-FDG PET/CT) is the best method for diagnosing tumors and guiding treatment. The standardized uptake value (SUV) is commonly used in clinics to estimate ^{18}F-FDG uptake in normal tissues and tumors. However, SUV is semi-quantitative, and its accuracy can be compromised by blood glucose concentration, dynamics of plasma ^{18}F-FDG, and the distribution of ^{18}F-FDG in the human body [1]. These factors can easily lead to false-positive results. A quantitative method can overcome the limitations of more routine methods. Consequently, more researchers recently investigate the utility of absolute quantitative dynamic imaging [2,3].

There are two methods to realize quantitative dynamic PET/CT imaging, including single- and multi-bed dynamic scanning. Single-bed dynamic imaging only adapts to regional imaging, whereas multi-bed dynamic scanning allows whole-body imaging. Arterial input function (AIF) and the influx rate constant Ki are the most important factors in ^{18}F-FDG PET/CT absolute quantitative dynamic multi-bed imaging. The AIF consists of blood time-activity curves (TAC) and can be acquired invasively by continuously phlebotomizing from an artery, a procedure that most patients are unable or unwilling to undergo [4], or nonin-

Correspondence to: Rong-fu Wang, MD, PhD. Department of Nuclear Medicine, Peking University First Hospital, Xichengqu, West District, Beijing, P. R. of China. Tel: +86 1083572954, E-mail: wang-qiang1983@163.com
Received: 23/04/2013; Accepted: 08/05/2013

Table 1. Clinical features of the malignant and benign group

Features	*Malignant group mean±SD*	*Benign group mean±SD*	*p-value*
Age (years)	52.25±4.62	50.00±8.68	
Gender (male/female)	6/4	6/5	
Prior treatment	0	0	
Lesions	15	14	
Lesion maximum diameter (cm)	2.993±1.25	2.821±1.22	>0.05
SUV_{max}	2.793±0.47	2.294±0.68	<0.05
Ki values (KBq/mL)	0.325±0.22	0.116±0.18	<0.05

SD: standard deviation

vasively, as done in this study. An image-derived input function (IDIF) has been developed and validated as a noninvasive technique in quantitative dynamic multi-bed imaging [5,6]. At present, most researchers utilize the left ventricular blood pool and aorta for IDIF. Both the two-tissue-compartment model and Patlak plot methods require AIF and tissue TAC to generate Ki. The two-tissue-compartment model is a standard method in dynamic multi-bed imaging, but its calculation is complex. Patlak plots neglect the process of dephosphorylation because the levels of glucose 6-phosphatase in myocardium, tumor, brain, and inflammatory lesions are near zero [7]. Therefore, the calculation of a Patlak plot analysis is simple, and easy to generate a parametric image.

The clinical identification and diagnosis of pulmonary lesions is always difficult. Most researchers advocate SUV_{max}>2.5 as important positive evidence for the diagnosis of a malignant pulmonary lesion [8,9]. However, some benign pulmonary lesions may have a SUV_{max}>2.5 (e.g., inflammatory granuloma and pulmonary tuberculosis) [9].

The following new quantitative PET/CT dynamic multi-bed imaging technology study may facilitate the identification of benign lung lesions and could potentially prevent false-positive imaging in cases with SUV_{max}>2.5.

Methods

Patients

Twenty-one patients with pulmonary lesions underwent ^{18}F-FDG PET/CT dynamic multi-bed imaging and a routine examination in our hospital. No patient had history of diabetes or heart disease. None of the patients had any treatment prior to PET/CT examination, and they were divided into malignant and benign groups. The malignant group had 10 patients with 15 lesions; 8/15 lesions were from primary lung cancer and 7/15 metastases to the lung. The benign group had 11 patients with 14 lesions; 4/14 were inflammatory granuloma, 3/14 tuberculosis and 7/14 inflammatory lesions. All pulmonary lesions were confirmed pathologically and by 6-month follow-up. Patient and tumor clinical characteristic are listed in Table 1.

The experimental protocol was approved by the clinical research ethics committee at the Peking University First Hospital. All patients provided written informed consent.

^{18}F-FDG PET/CT dynamic multi-bed imaging and routine scan

All patients fasted for at least 6 h, and blood sugar, height, and weight were measured before performing PET/CT scan. The radiochemical purity of ^{18}F-FDG was over 95%, and the injected dose ranged from 233.1 to 307.1MBq. The mean value of the injected dose was 258.8±23.4MBq.

The dynamic whole-body ^{18}F-FDG PET data acquisition protocol was implemented on a Philips Gemini GXL 16 PET-CT (Philips Medical Systems, Cleveland, OH). Patients laid with their arms up to ensure that their heart was positioned in the PET field of view (FOV). First, the CT scan (120keV and 10mA) was performed before ^{18}F-FDG injection for attenuation correction, and the ^{18}F-FDG injection point was defined as time 0. Immediately after the intravenous bolus injection of ^{18}F-FDG, 6 min of three-dimensional (3D) list mode in the dynamic PET/CT scan began with over 20 frames (18×20s) with the patient's heart located in the center of the FOV. Finally, a PET systemic six-sequence whole-body scan was performed with 30sec/bed only in the cranial to caudal direction. The time of the entire ^{18}F-FDG PET/CT dynamic multi-bed scan was approximately 60 min. Afterwards, patients underwent a routine PET/CT scan with 90sec/bed from foot to head that took approximately 12 min. All dynamic multi-bed imaging and routine scan data were reconstructed with 2D modes and corrected for attenuation, dead time, and random coincidences.

Arterial input function

The non-invasive plasma AIF estimation technique was used to facilitate clinical acceptance. The left ventricular (LV) pool is the largest blood pool that allows minimized partial volume effects. Therefore, we adopted the LV blood pool for IDIF, continuously at the early stage of the scan and sparsely in subsequent multi-bed passes through the heart. The region of interest (ROI) concerning the LV cavity was sketched, and overlap with the myocardium was avoided in order to prevent myocardial spillover effects. We took the max-

imum counts of ROI to generate the TAC. To avoid the bias of statistical noise, we sketched the ROI of six adjacent cross sections of the left ventricle and then generated average data, as shown in Figure 1.

Influx rate constant Ki

The Patlak plot is a graphical analysis approach that has been extensively validated for ^{18}F-FDG uptake rate constant estimation [10]. The Patlak plot method obtains Ki with the equation:

$$C_i(t) = Ki \int_0^t C_p(t)dt + V/C_p(t)$$

,where Ci(t) is tissue ^{18}F-FDG concentration change with time, Cp(t) is the plasma ^{18}F-FDG concentration change with time, V is the intercept of regression comprised of the effective plasma volume and the distribution of volume of reversible compartments, and Ki is the slope of linear regression that equals the tissue ^{18}F-FDG influx or uptake rate constant. We utilized an adaptive Bayesian estimation framework that used the powerful theory of ridge regression to regularize linear regression. From the above equation, it can be seen that Ki measures the changes of tissue concentration normalized with respect to the time-course of plasma ^{18}F-FDG, while SUV-based metrics measure tissue concentration without considering plasma ^{18}F-FDG dynamics.

Analysis of pulmonary lesions and parameter estimation

Three experienced nuclear medicine physicians assessed the PET/CT images. The pulmonary lesions were sketched, and the Patlak plot was used to generate Ki and parametric images. The parametric images generated by conventional linear regression or nonlinear regression methods for multi-bed ^{18}F-FDG PET data are too noisy for routine clinical use. Members from our team demonstrated that spatial-constraints based on parametric imaging algorithms can be used to modify dynamic multi-bed ^{18}F-FDG PET/CT imaging and remarkably reduce the noise in parametric Ki images [11,12]. At the same time, the pulmonary lesions of routine PET/CT images were analyzed to obtain SUV_{max} for comparison with Ki.

Influx rate constant Ki estimation of dynamic multi-bed PET data was done with the PMOD software package (version2.75, Technologies Ltd., Zurich, Switzerland), which was provided by Johns Hopkins University.

Statistics

All data were analyzed by SPSS 17.0 (SPSS Inc., Chicago, IL, USA). Quantitative data were expressed as mean±standard deviation (SD). Lesion maximum diameter, influx rate constant Ki and SUV_{max} obtained in both groups were analyzed by Wilcoxon-Mann-Whitney U tests, and $p<0.05$ was considered statistically significant. The correlation of Ki values and SUV_{max} were analyzed with Spearman test.

Results

The TAC of malignant pulmonary lesions demonstrated gradual increases in ^{18}F-FDG uptake until 60 min, whereas benign lesions exhibited gradual decreases in TAC over 60 min (Figure 1). Typical TAC and Ki parametric images for malignant and benign lesions are shown in Figures 2 and 3, respectively.

The maximal lesion diameter was not significantly different between groups ($p>0.05$). Malignant pulmonary lesions demonstrated significantly higher Ki values ($p<0.05$) and SUV_{max} ($p<0.05$) than benign lesions. All 15 malignant lesions had SUV_{max} values > 2.5. We found that 10 (out of 14) benign lesions had SUV_{max} values < 2.5, and the remaining 4 benign lesions had SUV_{max} values > 2.5 but gradually decreased activity on TAC, as shown in Figure 3. The Ki values were significantly correlated with SUV_{max} values in pulmonary le-

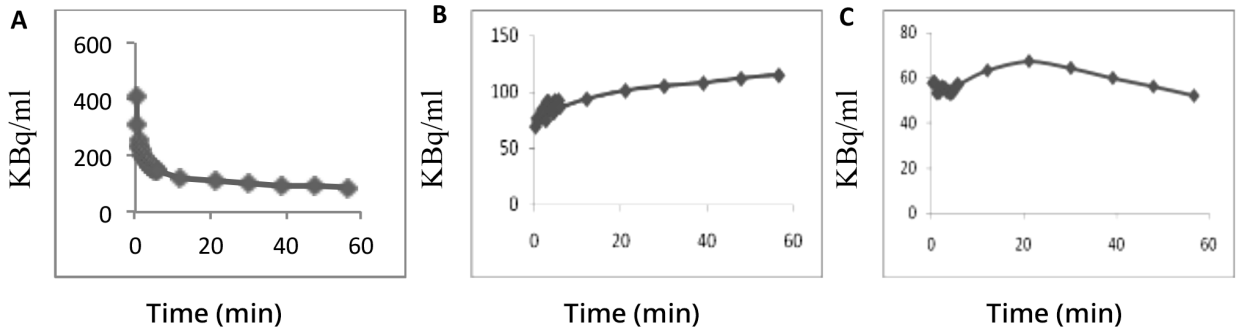

Figure 1. (A) Mean arterial input function for 21 patients generated by image-derived input function. **(B)** Mean time-activity curves for 10 patients with 15 malignant pulmonary lesions. **(C)** Mean time-activity curves for 11 patients with 14 benign pulmonary lesions.

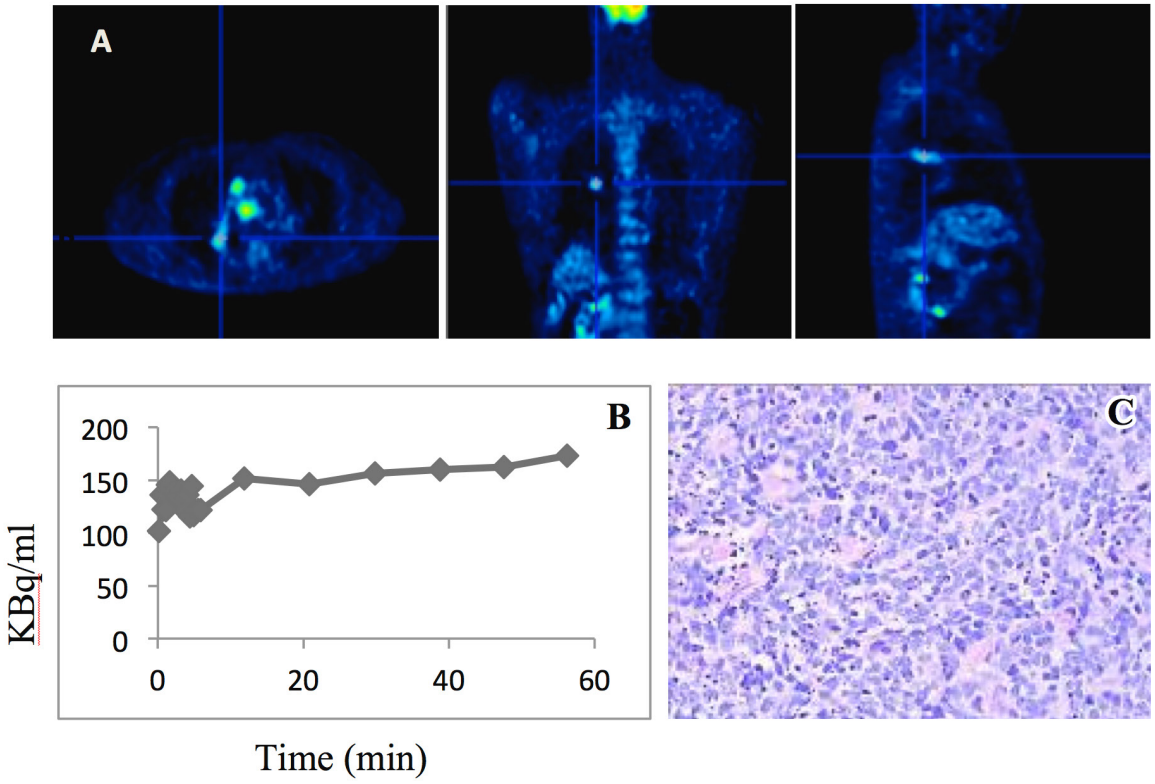

Figure 2. (A) A lesion in the right lung in a 56-year-old man is evident with Ki parametric imaging (left: transverse, middle: coronal, right: median sagittal). **(B)** The SUV_{max} and Ki of this lesion were 3.7 and 0.616 kBq/mL, respectively. The TAC of this lesion gradually increased over 60 min. **(C)** Microscopic examination with hematoxylin and eosin (×40) shows a small cell lung cancer lesion.

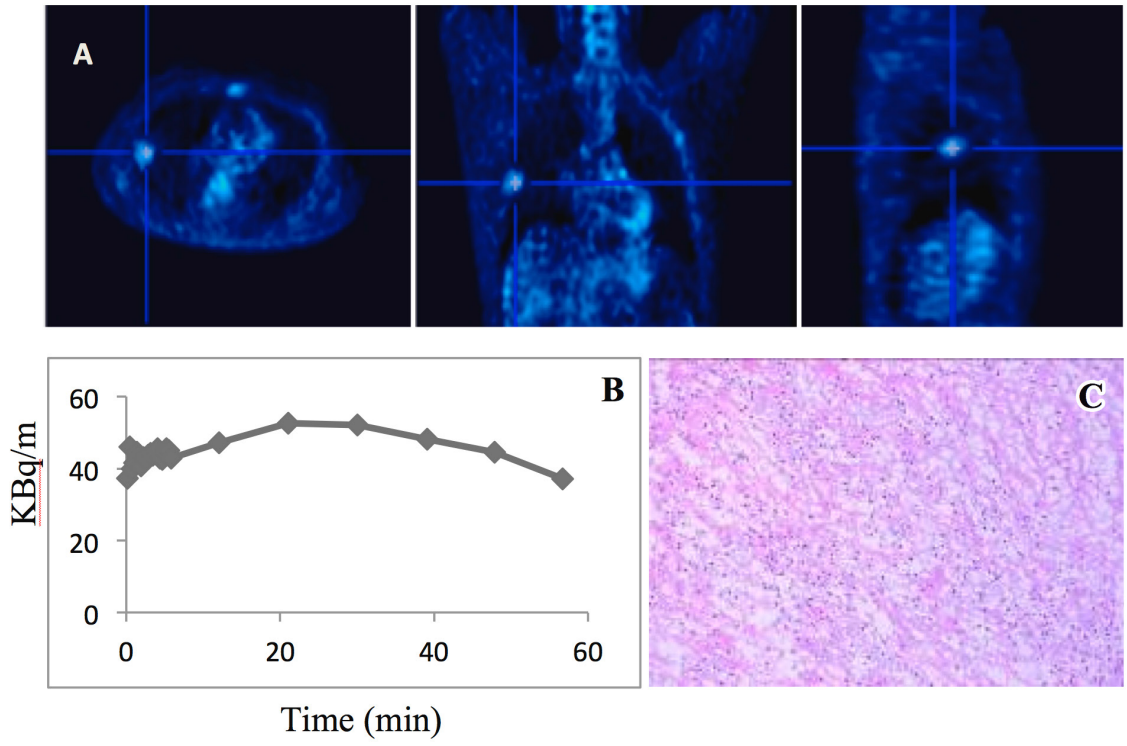

Figure 3. (A) A 40-year-old man with a lesion in the right lung which is evident with Ki parametric imaging (left: transverse, middle: coronal, right: median sagittal). **(B)** The SUV_{max} and Ki of this lesion are 3.8 and 0.231 kBq/mL, respectively. The TAC of this lesion gradually decreases over 60 min. **(C)** Microscopic examination with hematoxylin and eosin (×20) shows an inflammatory granulomatous lesion.

sions (r=0.815, p<0.01). The inter-group differences in maximum lesion diameter, Ki, and SUV_{max} are shown in Table 1.

Discussion

Tissue metabolism is susceptible to blood levels of insulin; therefore, diabetics should take measures to control their blood glucose levels before undergoing ^{18}F-FDG PET/CT scanning. The best noninvasive method to acquire AIF is IDIF and requires rapid PET data acquisition. Therefore, this method can only be applied to the LV and the aorta [13,14]. We selected the LV for IDIF because the LV sketch was easier than the aorta, and the LV has the largest blood pool. Cardiac dysfunction may impair heart contraction and relaxation, thereby affecting the radioactive count of the LV. None of the patients included in this study had a history of diabetes or heart disease.

The two-tissue-compartment model and the Patlak plot are the most important methods for generating the influx rate constant Ki. The two-tissue-compartment model makes use of AIF and tissue TAC from 0 to 60 min to generate k1-k4 and calculate Ki. The rate constant values k1, k2, k3, and k4 represent the course of ^{18}F-FDG forward transport, reverse transport, phosphorylation, and dephosphorylation, respectively [15,16]. The Ki was calculated as shown in the following equation Ki=k1k3/(k2+k3). The Patlak plot method assumes that k4 is zero and uses the linear regression diagram to generate Ki. We also made use of spatial-constraint-based parametric imaging algorithms to improve Ki parametric images. The Patlak plot has many advantages over the two-tissue-compartment model. The calculation of this method is simpler and is not susceptible to the influence of image noise [16,17].

^{18}F-FDG PET/CT has been widely used to detect and diagnose tumors, especially pulmonary lesions. In most cases, SUV_{max} is considered a reliable method in the differentiation between benign and malignant lesions. In our study, malignant pulmonary lesions demonstrated significantly higher SUV_{max} (p<0.05) than benign lesions, and the maximum diameters of the two types of lesions were not significantly different (p>0.05). The majority of benign lesions had SUV_{max} values < 2.5, whereas the SUV_{max} values of most malignant lesions were > 2.5. Therefore, SUV_{max}>2.5 can be considered a criterion for the differential diagnosis of benign and malignant lesions. However, SUV is a semi-quantitative method that is easily affected by many factors, such as plasma glucose levels and ^{18}F-FDG distribution and clearance [18]. In addition, benign and malignant lesions can overlap. Some benign lesions can also have a SUV max>2.5, which can lead to false-positive imaging. Dual-time-phase is a useful method for differentiating between benign and malignant lesions at two points, usually at 60 and 120 min. However, some studies have shown that the dual-time-phase method cannot differentiate between some lesions, including benign and malignant pulmonary lesions [19-21]. This is especially true for solitary pulmonary lesions. ^{18}F-FDG PET/CT dynamic multi-bed imaging as an absolute quantitative method can reflect the organization of cell metabolism. Therefore, dynamic imaging can contribute to the diagnosis of benign or malignant lesions and help avoid false-positive imaging.

The false-positive imaging diagnosis of malignant pulmonary lesions is mainly due to the existence of benign lesions that also take up ^{18}F-FDG; SUV_{max} can be > 2.5 in these lesions. In our study, the SUV_{max} of 4 benign lesions was > 2.5. Inflammatory cell infiltration explains high SUV_{max} values of some benign lesions, such as tuberculosis, inflammatory granuloma, and bacterial infection [22]. These inflammatory lesions are rich in inflammatory cells, such as macrophages, lymphocytes, and eosinophils that express high levels of glucose transporter 1 (Glut-1), and hexokinase-like malignant lesions [23]. Therefore, these benign lesions can take up ^{18}F-FDG that can lead to a SUV_{max}>2.5. We investigated quantitative dynamic multi-bed Ki parametric imaging to identify a solution to the above-mentioned limitations of SUV-based approaches.

In our study, the TAC of 15 malignant lesions gradually rose during the dynamic scans, whereas those of 14 benign lesions gradually fell. The influx rate constant Ki showed higher values in malignant lesions compared to benign lesion (p<0.05), which may reflect different cellular structures. Theoretically, SUV_{max} is correlated with Ki, but this correlation may be affected by the false-positive or negative results of SUV-based imaging. In our study, the SUV_{max} values of 4 benign lesions were > 2.5, showing a significant correlation between Ki and SUV_{max} (r=0.815, p<0.01).

The use of dynamic ^{18}F-FDG PET studies and PET parametric images can be particularly useful for the detection and characterization of small lesions in the oropharynx, lung, liver, and pancreas. Despite its utility, dynamic PET imaging has been primarily confined to research centers and has not been used in busy clinical settings main-

ly due to limitations of the dynamic scanning [24]. For example, dynamic multi-bed scanning examination takes a long time. In addition, the method to obtain Ki requires further optimization. Other limitations include the lack of large clinical studies and the possibility of unreliable results in patients with heart disease or diabetes. However, ^{18}F-FDG PET/CT dynamic multi-bed scanning is theoretically better than SUV-based imaging. Routine clinical PET/CT imaging application could benefit from a translation of the above-mentioned quantitative methods to the clinical domain for the differential diagnosis of pulmonary lesions.

In conclusion, with absolute quantification of the metabolic state of tissue, multi-bed PET/CT dynamic imaging has the potential capability in differentiating benign from malignant lung lesions, although the number of patients in our study was limited.

Acknowledgements

This work was supported by grants from the Natural Science Foundation of China (NSFC 81071183), the Ministry of Science and Technology of China (projects 2011YQ030114 and 2011YQ03011409), the Research Fund for the Medicine and Engineering of Peking University (Fund BMU20120297), as well as the Research Fund (110204, 120121) of Key Laboratory of Radiopharmaceuticals (Beijing Normal University), Ministry of Education, Department of Chemistry, Beijing Normal University, Beijing, 100875, China.

We thank Li-Xiao Luo, engineer of Philips Corporation of China, who provided great technological support for this study.

References

1. Wu HM, Hoh CK, Huang SC et al. Quantification of serial tumor glucose metabolism. J Nucl Med 1996;37:506-513.
2. Messa C, Choi Y, Hoh CK et al. Quantification of glucose utilization in liver metastases:parametric imaging of FDG uptake with PET. J Comput Assist Tomogr 1992;16:684-689.
3. Castell F, Cook GJ. Quantitative techniques in ^{18}FDG PET scanning in oncology. Br J Cancer 2008;98:1597-1601.
4. Wu HM, Hoh CK, Choi Y et al. Factor analysis for extraction of blood time-activity curves in dynamic FDG-PET studies. J Nucl Med 1995;36:1714-1722.
5. Tsuchida T, Sadato N, Yonekura Y et al. Noninvasive measurement of cerebral metabolic rate of glucose using standardized input function. J Nucl Med 1999;40:1441-1445.
6. Dimitrakopoulou-Strauss A, Strauss LG, Heichel T et al. The role of quantitative ^{18}F-FDG PET studies for the differentiation of malignant and benign bone lesions. J Nucl Med 2002;43:510-518.
7. Freedman NM, Sundaram SK, Kurdziel K et al. Comparison of SUV and Patlak slope for monitoring of cancer therapy using serial PET scans. Eur J Nucl Med Mol Imaging 2003;30:46-53.
8. Bural G, Torigian DA, Houseni M et al. Tumor metabolism measured by partial volume corrected standardized uptake value varies considerably in primary and metastatic sites in patients with lung cancer. A new observation. Hell J Nucl Med 2009;12:218-222.
9. Lin M, Ambati C. The management impact of clinically significant incidental lesions detected on staging FDG PET-CT in patients with non-small cell lung cancer (NSCLC):an analysis of 649 cases. Lung Cancer 2012;76:344-349.
10. Zhou Y, Ye W, Brasić JR et al. Multi-graphical analysis of dynamic PET. Neuroimage 2010;49:2947-2957.
11. Zhou Y, Huang SC, Bergsneider M et al. Improved parametric image generation using spatial-temporal analysis of dynamic PET studies. Neuroimage 2002;15:697-707.
12. Zhou Y, Endres CJ, Brasić JR et al. Linear regression with spatial constraint to generate parametric images of ligand-receptor dynamic PET studies with a simplified reference tissue model. Neuroimage 2003;18:975-989.
13. Meyer PT, Circiumaru V, Cardi CA et al. Simplified quantification of small animal [^{18}F]FDG PET studies using a standard arterial input function. Eur J Nucl Med Mol Imaging 2006;33:948-954.
14. Zasadny KR, Wahl RL. Enhanced FDG-PET tumor imaging with correlation-coefficient filtered influx-constant images. J Nucl Med 1996;37:371-374.
15. Liu P, Huang G, Dong S et al. Kinetic analysis of experimental rabbit tumour and inflammation model with ^{18}F-FDG PET/CT. Nuklearmedizin 2009;48:153-158.
16. Hawkins RA, Choi Y, Huang SC et al. Quantitating tumor glucose metabolism with FDG and PET. J Nucl Med 1992;33:339-344.
17. Pavlopoulos S, Thireou T, Kontaxakis G et al. Analysis and interpretation of dynamic FDG PET oncological studies using data reduction techniques. Biomed Eng Online 2007;6:36.
18. Kamasak ME, Bouman CA, Morris ED et al. Direct reconstruction of kinetic parameter images from dynamic PET data. IEEE Trans Med Imaging

2005;24:636-650.

19. Ibeas P, Cantos B, Gasent JM et al. PET-CT in the staging and treatment of non-small-cell lung cancer. Clin Transl Oncol 2011;13:368-377.
20. Thomson D, Hulse P, Lorigan P et al. The role of positron emission tomography in the management of small cell lung cancer. Lung Cancer 2011;73:121-126.
21. Dong J, Su SY, Wang MY et al. Shenqi fuzheng, an injection concocted from Chinese medicinal herbs, combined with platinum-based chemotherapy for advanced non-small cell lung cancer:a systematic review. J Exp Clin Cancer Res 2010;22:137.
22. Muzi M, O'Sullivan F, Mankoff DA et al. Quantitative assessment of dynamic PET imaging data in cancer imaging. Magn Reson Imaging 2012;30:1203-1215.
23. Isbell JM, Deppen S, Putnam JB Jr et al. Existing general population models inaccurately predict lung cancer risk in patients referred for surgical evaluation. Ann Thorac Surg 2011;91:227-223.
24. Kwee TC, Basu S, Cheng G et al. FDG PET/CT in carcinoma of unknown primary. Eur J Nucl Med Mol Imaging 2010;37:635-644.